Neurobiology of Disease 169 (2022) 105742

Contents lists available at ScienceDirect

Neurobiology of Disease

journal homepage: www.elsevier.com/locate/ynbdi

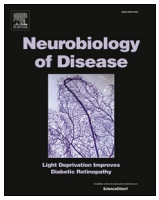

Somatosensory cortex hyperconnectivity and impaired whisker-dependent responses in *Cntnap2*$^{-/-}$ mice

Luigi Balasco [a], Marco Pagani [b], Luca Pangrazzi [a], Gabriele Chelini [a], Francesca Viscido [a], Alessandra Georgette Ciancone Chama [a], Alberto Galbusera [b], Giovanni Provenzano [c], Alessandro Gozzi [b], Yuri Bozzi [a,d,*]

[a] Center for Mind/Brain Sciences - CIMeC, University of Trento, Piazza della Manifattura 1, 38068 Rovereto, TN, Italy
[b] Functional Neuroimaging Laboratory, Center for Neuroscience and Cognitive Systems, Istituto Italiano di Tecnologia, Corso Bettini 31, 38068 Rovereto, Italy
[c] Department of Cellular, Computational, and Integrative Biology (CIBIO), University of Trento, via Sommarive 9, 38123 Trento, Italy
[d] CNR Neuroscience Institute, via Moruzzi 1, 56124 Pisa, Italy

ARTICLE INFO

Keywords:
Autism
Somatosensory
Connectivity
Gene expression

ABSTRACT

Sensory abnormalities are a common feature in autism spectrum disorders (ASDs). Tactile responsiveness is altered in autistic individuals, with hypo-responsiveness being associated with the severity of ASD core symptoms. Similarly, sensory abnormalities have been described in mice lacking ASD-associated genes. Loss-of-function mutations in *CNTNAP2* result in cortical dysplasia-focal epilepsy syndrome (CDFE) and autism. Likewise, *Cntnap2*$^{-/-}$ mice show epilepsy and deficits relevant with core symptoms of human ASDs, and are considered a reliable model to study ASDs. Altered synaptic transmission and synchronicity found in the cerebral cortex of *Cntnap2*$^{-/-}$ mice would suggest a network dysfunction. Here, we investigated the neural substrates of whisker-dependent responses in *Cntnap2*$^{+/+}$ and *Cntnap2*$^{-/-}$ adult mice. When compared to controls, *Cntnap2*$^{-/-}$ mice showed focal hyper-connectivity within the primary somatosensory cortex (S1), in the absence of altered connectivity between S1 and other somatosensory areas. This data suggests the presence of impaired somatosensory processing in these mutants. Accordingly, *Cntnap2*$^{-/-}$ mice displayed impaired whisker-dependent discrimination in the textured novel object recognition test (tNORT) and increased c-*fos* mRNA induction within S1 following whisker stimulation. S1 functional hyperconnectivity might underlie the aberrant whisker-dependent responses observed in *Cntnap2*$^{-/-}$ mice, indicating that *Cntnap2* mice are a reliable model to investigate sensory abnormalities that characterize ASDs.

1. Introduction

Abnormal sensory processing has been reported to occur in 90% of people diagnosed with autism spectrum disorders (ASDs) (Robertson and Baron-Cohen, 2017). Several studies point to altered processing of sensory information as a crucial feature of these disorders (Balasco et al., 2019), and both hyper- and hypo-reactivity to sensory stimuli are currently recognized as diagnostic criteria for ASD (American Psychiatric Association, 2013). Sensory abnormalities encompass all the sensory modalities, with the tactile domain being one of the most affected (Balasco et al., 2019). Abnormal sensory reactivity represents a crucial issue in autism research since it likely contributes to other ASD symptoms such as anxiety, stereotyped behaviors, as well as cognitive and social dysfunctions (Ben-Sasson et al., 2007; Sinclair et al., 2017), Interestingly, hypo-responsiveness to tactile stimulation has been found to positively correlate with severity of ASD core symptoms (Foss-Feig et al., 2012) and touch avoidance behavior in toddlers is predictive of ASD diagnosis later on in life (Mammen et al., 2015).

Abbeviations: ANOVA, analysis of variance; Amy, amygdala; ASD, autism spectrum disorder; BOLD, blood oxygenation level dependent; CDFE, cortical dysplasia-focal epilepsy syndrome; CNTNAP2, contactin associated protein-like 2; E/I, excitation/inhibition; EPI, echo planar imaging; G, grit; GABA, g-aminobutyric acid; GAD, glutamic acid decarboxylase; M Ctx, motor cortex; L, cortical layer; Mtn, medial thalamic nuclei; rsfMRI, resting-state functional magnetic resonance imaging; OF, open field; S1, primary somatosensory cortex; Pvalb, parvalbumin; TE, echo time; TN, trigeminal nucleus; tNORT, textured novel object recognition; TR, repetition time; vGLUT, vesicular glutamate transporter; Vpm, ventro postero-medial nucleus; WS, whisker stimulation under anesthesia.

* Corresponding author at: Center for Mind/Brain Sciences – CIMeC, University of Trento, Piazza della Manifattura 1, 38068 Rovereto, TN, Italy.
E-mail address: yuri.bozzi@unitn.it (Y. Bozzi).

https://doi.org/10.1016/j.nbd.2022.105742
Received 10 March 2022; Received in revised form 16 April 2022; Accepted 21 April 2022
Available online 26 April 2022

Mouse lines harboring ASD-relevant mutations have been recently used to assess the neurobiological underpinnings of abnormal sensory responses in ASD (Balasco et al., 2019; Orefice, 2020). Given the relevance of the whisker system in mice, the assessment of whisker-mediated behaviors represents an ideal proxy to study somatosensory processing defects (He et al., 2017; Chelini et al., 2019; Pizzo et al., 2020). Mice use their whiskers for a variety of behavior including object exploration (Brecht, 2007) and conspecific interaction (Ahl, 1986), and abnormalities in sensory perception through whiskers profoundly impact mouse behavior (Arakawa and Erzurumlu, 2015; Erzurumlu and Gaspar, 2020).

Research into the genetic bases of ASD has identified common and rare mutations in the *CNTNAP2* (contactin associated protein-like 2) gene associated with increased susceptibility to autism and schizophrenia (Alarcón et al., 2008; Arking et al., 2008; Bakkaloglu et al., 2008). Moreover, a recessive nonsense mutation in *CNTNAP2* was originally reported to cause cortical dysplasia-focal epilepsy syndrome (CDFE), a rare disorder characterized by epileptic seizures, language regression, intellectual disability and autism (Strauss et al., 2006). *CNTNAP2* codes for CASPR2, a transmembrane protein of the neurexin superfamily involved in neuron-glia interactions and clustering of potassium channels in myelinated axons (Poliak et al., 1999; Poliak et al., 2003). *Cntnap2* is highly expressed in several adult brain regions, including cerebral cortex, hippocampus, striatum, and cerebellum (Peñagarikano et al., 2011). Interestingly, *Cntnap2* is expressed in primary sensory organs and in brain regions involved in sensory processing (Gordon et al., 2016), suggesting a role for the *Cntnap2* gene in sensory neurotransmission.

Mice lacking the *Cntnap2* gene (Poliak et al., 2003) are considered a reliable model with both construct and face validity for ASD (Peñagarikano et al., 2011). In keeping with *Cntnap2* expression pattern (Gordon et al., 2016), studies indicate that lack of *Cntnap2* results in sensory dysfunction. *Cntnap2*$^{-/-}$ mice display enhanced hypersensitivity to noxious and thermal stimuli applied to hindpaws, which has been related to enhanced excitability of dorsal root ganglion neurons (Dawes et al., 2018). Moreover, despite reports of intact firing rate and amplitude in cortical neurons of *Cntnap2*$^{-/-}$ mice (Peñagarikano et al., 2011), lack of *Cntnap2* has been shown to impair synaptic transmission in cortical neurons in vitro (Anderson et al., 2012) and layer 2/3 pyramidal neurons of the somatosensory cortex following whisker stimulation (Antoine et al., 2019). Circuit connectivity is also impaired in sensory cortical areas of *Cntnap2* mutant mice (Choe et al., 2021), suggesting a broad neuronal network remodeling in these mutants.

Here we investigated the effect of *Cntnap2* gene inactivation on somatosensory cortex connectivity and whisker-dependent responses at the behavioral and cellular level. We first used a seed-based approach in rsfMRI to probe functional connectivity alterations in the primary somatosensory cortex (S1) and other somatosensory areas of *Cntnap2* mutant mice. We next performed textured novel object recognition test (tNORT) and c-*fos* mRNA in situ hybridization to assess behavioral and cellular whisker-dependent responses in adult *Cntnap2*$^{-/-}$ and control mice. Our data reveal altered S1 functional connectivity and aberrant whisker-dependent responses in *Cntnap2*$^{-/-}$ mice.

2. Materials and methods

2.1. Animals

All experimental procedures were performed in accordance with Italian and European directives (DL 26/2014, EU 63/2010) and were reviewed and approved by the University of Trento animal care committee and Italian Ministry of Health. Animals were housed in a 12 h light/dark cycle with food and water available ad libitum. Surgical procedures were performed under anesthesia and all efforts were made to minimize suffering. *Cntnap2* mutants were crossed at least five times into a C57BL/6 background. Heterozygous mating (*Cntnap2*$^{+/-}$ x *Cntnap2*$^{+/-}$) was used to generate the *Cntnap2*$^{+/+}$ and *Cntnap2*$^{-/-}$ littermates used in this study. PCR genotyping was performed according to the protocol available on The Jackson Laboratory website (www.jax.org). A total of 101 age-matched adult littermates (50 *Cntnap2*$^{+/+}$ and 51 *Cntnap2*$^{-/-}$; 3–6 months old; weight = 25–35 g) of both sexes were used. The stage of the estrous cycle was not monitored for female animals used in this study. Twenty-six mice (13 *Cntnap2*$^{+/+}$ and 13 *Cntnap2*$^{-/-}$) were used for fMRI experiments. Fifty-three mice (26 *Cntnap2*$^{+/+}$ and 27 Cntnap2$^{-/-}$) were used for the open field test. A subset of 30 animals (15 *Cntnap2*$^{+/+}$ and 15 *Cntnap2*$^{-/-}$) also performed the textured novel object recognition test (tNORT). Twelve mice were used for c-*fos* mRNA in situ hybridization (6 *Cntnap2*$^{+/+}$ and 6 *Cntnap2*$^{-/-}$) following either anesthesia or whisker stimulation. Finally, 10 animals (5 *Cntnap2*$^{+/+}$ and 5 *Cntnap2*$^{-/-}$) were used in the RT-qPCR study (see Fig. 1 for a summary of the experimental scheme). Previous studies showed that similar group sizes are sufficient to obtain statistically significant results in fMRI, behavioral, and in situ hybridization studies (Balasco et al., 2021). All experiments were performed blind to genotype. Animals were assigned a numerical code by an operator who did not take part in the experiments and codes were associated to genotypes only at the moment of data analysis.

2.2. Resting-State Functional MRI (rsfMRI)

rsfMRI time-series were recorded in male *Cntnap2*$^{-/-}$ ($n = 13$, 13–14 weeks old) and age-matched *Cntnap2*$^{+/+}$ control littermates (n = 13) as described (Liska et al., 2018). Briefly, animals were anesthetized with isoflurane (5% induction), intubated and artificially ventilated (2% maintenance). After surgery, isoflurane was discontinued and replaced with halothane (0.75%). Recordings started 45 min after isoflurane cessation. Functional scans were acquired with a 7 T MRI scanner (Bruker Biospin, Milan) using a 72-mm birdcage transmit coil and a 4-channel solenoid coil for signal reception. For each animal, in-vivo anatomical images were acquired with a fast spin echo sequence (repetition time [TR] = 5500 ms, echo time [TE] = 60 ms, matrix 192 × 192, field of view 2 × 2 cm, 24 coronal slices, slice thickness 500 μm). Co-centered single-shot BOLD rsfMRI time series were acquired using an echo planar imaging (EPI) sequence with the following parameters: TR/TE 1200/15 ms, flip angle 30°, matrix 100 × 100, field of view 2 × 2 cm, 24 coronal slices, slice thickness 500 μm for 500 volumes.

2.3. Functional connectivity analyses

Resting state functional MRI connectivity is a method to map spatiotemporal synchronization of spontaneous BOLD fluctuations across brain regions and is widely used in human clinical (Di Martino et al., 2014) and rodent (Pagani et al., 2021; Zerbi et al., 2021) studies to describe alterations of brain networks in autism and other neuropsychiatric disorders. Functional connectivity analyses reported here were carried out on the rsfMRI scans acquired for our previous study (Liska et al., 2018). Here we used seed-based correlation mapping to probe putative functional connectivity alterations associated to *Cntnap2* homozygous mutation. Before mapping rsfMRI connectivity, raw time-series were pre-processed and denoised as previously described (Liska et al., 2018; Coletta et al., 2020). First, the initial 50 volumes were removed to allow for T1 equilibration effects. Time series were then despiked, motion corrected and registered (Pagani et al., 2016) to a common group-averaged BOLD reference template. Motion traces of head realignment parameters and mean ventricular signal were then used as nuisance covariates and regressed out from each time course. Before functional connectivity mapping, all time-series underwent band-pass filtering (0.01–0.1 Hz) and spatial smoothing (FWHM = 0.6 mm). Functional connectivity of brain regions associated with whisker-mediated behaviors were mapped using seed-based correlation analysis. Specifically, bilateral seeds of 3 × 3 × 1 voxels were placed in the primary somatosensory (S1) cortex and ventral postero-medial nucleus

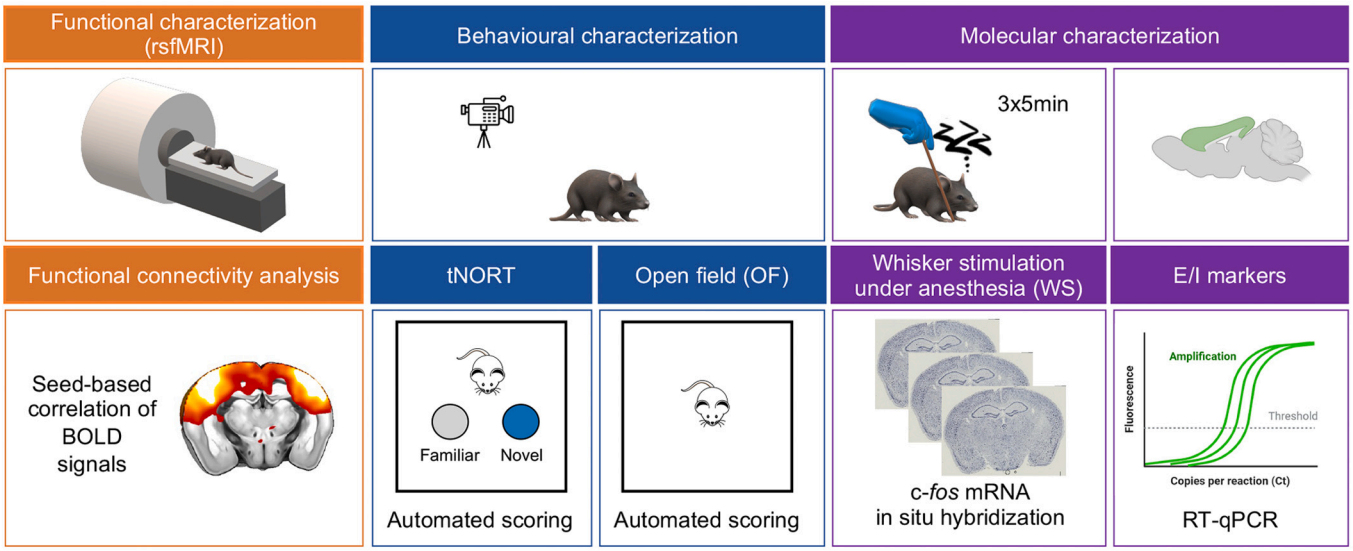

Fig. 1. Experimental paradigm on *Cntnap2*$^{+/+}$ and *Cntnap2*$^{-/-}$ adult mice of both sex. Functional connectivity analysis was performed with seed-based correlation of BOLD signals in S1. Functional characterization was performed via rsfMRI. Behavioral characterization consisted in the textured novel object recognition test (tNORT) and open field test (OF). Behavioral data were acquired through automated software (Ethovision). Molecular characterization of neuronal activity was performed via c-*fos* in situ hybridization (ISH) following whisker stimulation under anesthesia (WS) and quantitative real-time PCR (qRT-PCR) on excitation/inhibition markers in neocortex. Molecular data consisted in mRNA signal intensity calculated in S1 through Fiji software from ISH experiments and expression data from gene analysis study.

(VPM) of the thalamus of *Cntnap2*$^{-/-}$ and *Cntnap2*$^{+/+}$ mice to probe functional connectivity between these regions and the rest of the brain. The location of the bilateral seeds employed for mapping is indicated in Fig. 2. Functional connectivity was measured with Pearson's correlation and r-scores were transformed to z-scores using Fisher's r-to-z transform before group-level statistics. Voxel-wise intergroup differences for seed-based mapping were assessed using a 2-tailed Student's *t*-test ($t > 2$, $p < 0.05$) and family-wise error (FWER) cluster-corrected using a cluster threshold of $p = 0.01$. To quantify rsfMRI alterations we also carried out functional connectivity measures in cubic regions of interest ($3 \times 3 \times 1$ voxels). The statistical significance of these region-wise intergroup effects was quantified using a 2-tailed Student's t-test ($t > 2$, $p < 0.05$).

2.4. Textured novel object recognition test (tNORT)

Whisker-mediated texture discrimination was assed as described (Wu et al., 2013; Balasco et al., 2021). Since mice have an innate preference for novel stimuli, an animal that can discriminate between the textures of the objects spends more time investigating the novel textured object, whereas an animal that cannot discriminate between the textures is expected to investigate the objects equally. Experiments were performed in a standard open field arena (40 cm × 40 cm × 40 cm) containing two cylinder-shaped objects (1.5 cm radius base x 12 cm height) covered in garnet sandpaper. The grit (G) of the objects (i.e., how rough the sandpaper is) was chosen according to Wu et al. (2013), to favor whisker interaction. A 120 G sandpaper (fine texture) was used for the familiar object, whereas 40 G sandpaper (coarse texture) was used for the novel object. Many identical objects were created for each grit of sandpaper to avoid recognition via olfactory cues. Moreover, the test was performed in penumbra (4 lx) to avoid possible visual confounds. Adult mice have a very low visual acuity (Schmucker et al., 2005), which does not allow them to discriminate the grit of the two objects at this light intensity. The test started after two days of habituation in the arena. In the first session (learning phase), mice were placed in the testing arena facing away from two identically textured objects (object A and object B; 120 G) and allowed to freely explore the objects for 5 min. This short time was selected to favor the investigation through whiskers. The textured objects were placed in the center of the arena, equidistant to each other and the walls. Mice were then removed and held in a separate transport cage for 5 min. This short time was selected to minimize hippocampal mediated learning (Wu et al., 2013; Balasco et al., 2021). Prior to the start of the second session, the two objects in the arena were replaced with a third, identically textured object (familiar, 120 G) and a new object with a different texture (novel, 40 G). The position of the novel versus the familiar object was counterbalanced and pseudorandomized (i.e, the position of the two objects was exchanged between each mouse and the following one). Mice were then placed back into the arena for the second session (testing phase) and allowed to explore for 5 min. The testing arena was cleaned with 70% ethanol between sessions and between animals to mask olfactory cues. The amount of time mice spent actively investigating each of the objects was assessed during both learning and testing phases. Investigation through whiskers was defined as directing the nose towards the object with a distance of less than 2 cm from the nose to the object or touching the nose to the object. Resting, grooming, and digging next to, or sitting on, the object was not considered as an investigation. Mice that had a total investigation time of less than 2 s during either learning and testing phases were excluded from the analysis due to poor exploratory activity (Wu et al., 2013). The activity of the mice during the learning and testing phase was recorded with a video camera centered above the arena and automatically tracked using EthoVisionXT (Noldus). The performance of the mice in the tNORT was expressed by the preference index. The preference index is the ratio of the amount of time spent exploring any one of the two objects in the learning phase or the novel one in the testing phase over the total time spent exploring both objects, expressed as percentage [i.e., A/(B + A) × 100 in the learning session and novel/(familiar + novel) × 100 in the testing session].

2.5. Open field test

Animals were placed in an open field arena (40 cm × 40 cm × 40 cm) and allowed to freely explore for 10 min. The walls of the arena were smooth and grey colored. Sessions were recorded and mice were automatically tracked using EthoVisionXT (Noldus). Average speed, distance travelled and time spent in center/borders were analyzed.

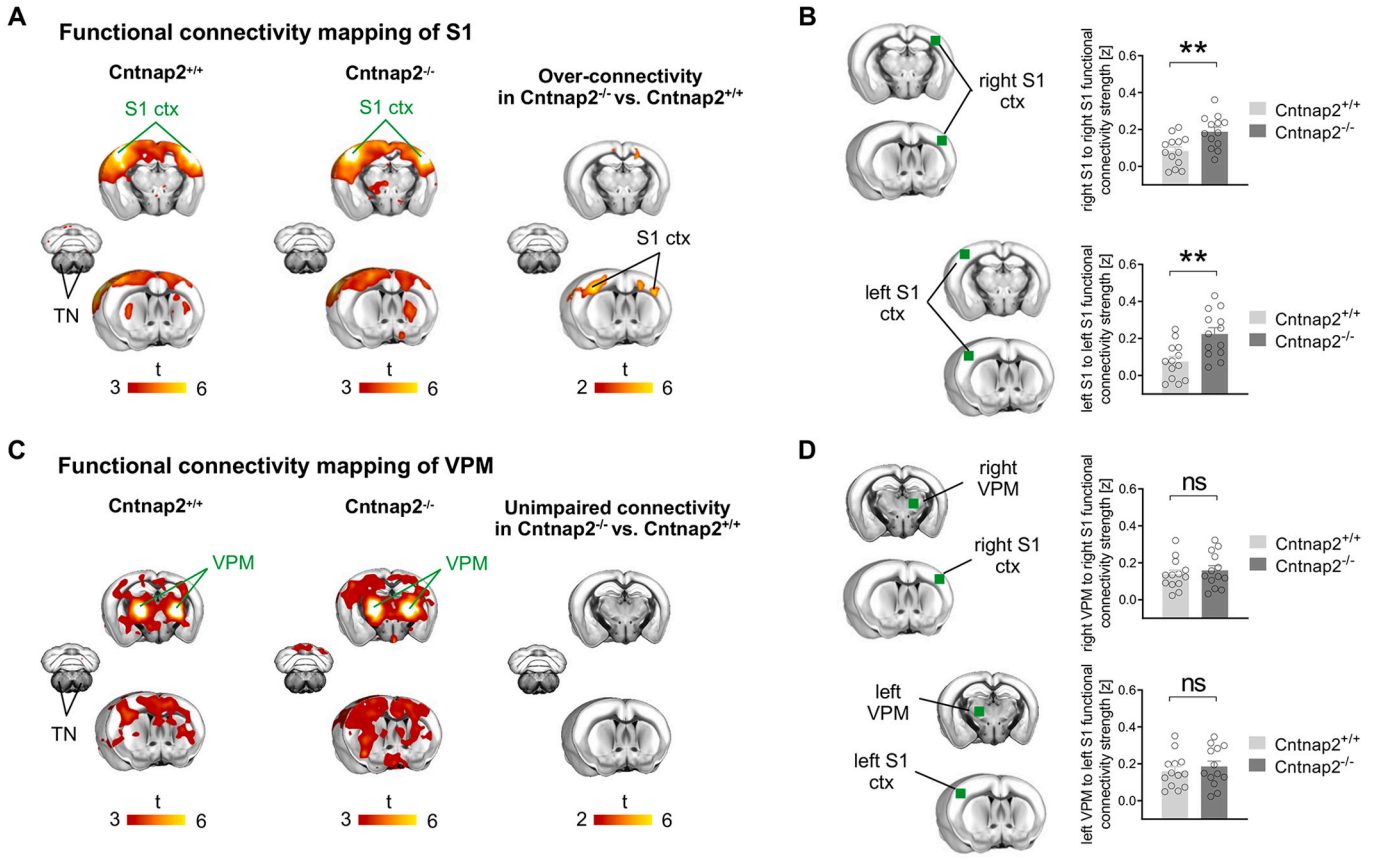

Fig. 2. Increased functional connectivity within the somatosensory cortex of *Cntnap2*$^{-/-}$ mice. (*A*) Seed-based connectivity maps of S1 cortex in *Cntnap2*$^{+/+}$ and *Cntnap2*$^{-/-}$ mice. Red-yellow represents brain regions showing significant rsfMRI functional connectivity with the S1 in *Cntnap2*$^{+/+}$ (left) and *Cntnap2*$^{-/-}$ mice (middle). Seed region is depicted in green lettering. Brain regions showing rsfMRI over-connectivity in *Cntnap2*$^{-/-}$ mice with respect to *Cntnap2*$^{+/+}$ control littermates are depicted in red-yellow (right). (*B*) Functional connectivity within the S1 was also quantified in unilateral reference volumes of interest (green). (*C*) Seed-based connectivity maps of the VPM. Red-yellow represents brain regions showing significant rsfMRI functional connectivity with the VPM in *Cntnap2*$^{+/+}$ (left) and *Cntnap2*$^{-/-}$ mice (middle). Seed region is depicted in green lettering. No change of rsfMRI connectivity of the VPM was detected in *Cntnap2*$^{-/-}$ mice with respect to *Cntnap2*$^{+/+}$ mice (right). (*D*). Functional connectivity between VPM and S1 was also quantified in unilateral reference volumes of interest (green). Error bars represent SEM. S1 ctx, primary somatosensory cortex; VPM, ventral posteromedial nucleus of the thalamus; TN, trigeminal nucleus. ** $p < 0.01$ (unpaired *t*-test, $n = 13$ *Cntnap2*$^{+/+}$ and n = 13 *Cntnap2*$^{-/-}$ mice, each dot represents one animal). (For interpretation of the references to colour in this figure legend, the reader is referred to the web version of this article.)

2.6. Whisker stimulation under anesthesia (WS)

Mice were anesthetized with an intraperitoneal injection of urethane (20% solution in sterile double-distilled water, 1.6 g/kg body weight) and head-fixed on a stereotaxic apparatus. Urethane anesthesia was chosen as it preserves whisker-dependent activity in the somatosensory cortex (Balasco et al., 2021). WS protocol consisted in 3 consecutive sessions (5 min each, with 1 min intervals) of continuous touch of the whiskers with a wooden stick (bilateral stimulation).

2.7. c-fos mRNA in situ hybridization

Mice were killed 20 min after the end of WS and anesthesia only sessions, and brains were rapidly frozen on dry ice. Coronal cryostat sections (20 μm thick) were fixed in 4% paraformaldehyde and processed for non-radioactive in situ hybridization using a digoxigenin-labelled c-*fos* riboprobe (Balasco et al., 2021). Signal was detected by alkaline phosphatase-conjugated anti-digoxigenin antibody followed by alkaline phosphatase staining. Brain sections were processed together for c-*fos* expression in order to exclude possible batch effects. Sense riboprobes, used as negative control, revealed no detectable signal (data not shown). Brain areas were identified according to the Allen Mouse Brain Atlas (https://mouse.brain-map.org). Digital images from 4 to 8 sections per animal were acquired at the level of the S1 and other brain regions of interest using a Zeiss AxioImager II microscope at 10× primary magnification.

2.8. Quantitative reverse transcription – polymerase chain reaction (RT-qPCR)

Total RNAs were extracted from the cerebral cortex of adult *Cntnap2*$^{+/+}$ and *Cntnap2*$^{-/-}$ mice, and retro-transcribed to cDNA according to manufacturer's protocol. qRT-PCR was performed in a CFX96™ Real-Time System (Bio-Rad, USA), using PowerUp™ SYBR™ Green Master Mix (ThermoFisher). Primers (Sigma) were designed on different exons to avoid amplification of genomic DNA (Table 1). The

Table 1
Primers used for quantitative RT-PCR experiments.

Gene	Forward (5′-3′)	Reverse (5′-3′)
β-Actin	AATCGTGCGTGACATCAAAG	AAGGAAGGCTGGAAAAGAGC
vGlut1	CCCCCAAATCCTTGCACTTT	AACAAATGGCCACTGAGAAACC
vGlut2	TGCTACCTCACAGGAGAATGGA	GCGCACCTTCTTGCACAAAT
Gad1	CGTGCATTTGTGAGCCAAAGA	ACATCTGACATACAGCTTGAG
Gad2	CATTCCTGTCCTTGCCTCTC	GTGCATCCTTTGTCCATGT
Pvalb	TGTCGATGACAGACGTGCTC	TTCTTCAACCCCAATCTTGC

CFX3 Manager 3.0 (Bio-Rad) software was used to perform expression analyses (Sgadò et al., 2013). Mean cycle threshold (Ct) values from replicate experiments were calculated for each marker and β-actin (used as a standard for quantification), and then corrected for PCR efficiency and inter-run calibration. The expression level of each mRNA of interest was then normalized to that of β-actin for both genotypes. For RT-qPCR experiments, the expression levels of each marker (normalized to that of β-actin) were compared from at least 4 replicate experiments performed on RNA pools from 5 animals per genotype. Statistical analysis was performed by unpaired *t*-test.

2.9. Statistical analyses

Statistical analyses of behavioral and in situ hybridization data were performed with GraphPad Prism 8.0 software, with the level of significance set at $p < 0.05$. For behavioral experiments, statistical analysis was performed by Mann-Whitney test or two/three-way ANOVA followed by Tukey's or Bonferroni's post-hoc multiple comparisons, as appropriate. To quantify mRNA signal intensity from in situ hybridization experiments, acquired images were converted to 8-bit (grey-scale), inverted, and analyzed using the ImageJ software (https://imagej.net/Downloads). Mean signal intensity was measured in different counting areas drawn to identify S1 cortical layers and other areas of interest. Mean signal intensity was divided by the background calculated in layer 1. Statistical analysis was performed by unpaired t-test.

3. Results

3.1. Functional over-connectivity within S1 in *Cntnap2*$^{-/-}$ mice

We previously reported that homozygous loss of *Cntnap2* leads to profoundly altered prefronto-cortical functional coupling (Liska et al., 2018). To investigate functional synchronization in somatosensory areas, we probed rsfMRI connectivity of S1 in *Cntnap2* mutants (Fig. 2*A*). Notably, voxelwise rsfMRI connectivity mapping of S1 revealed increased functional connectivity within S1 ($t > 2$, $p < 0.05$ and FWER

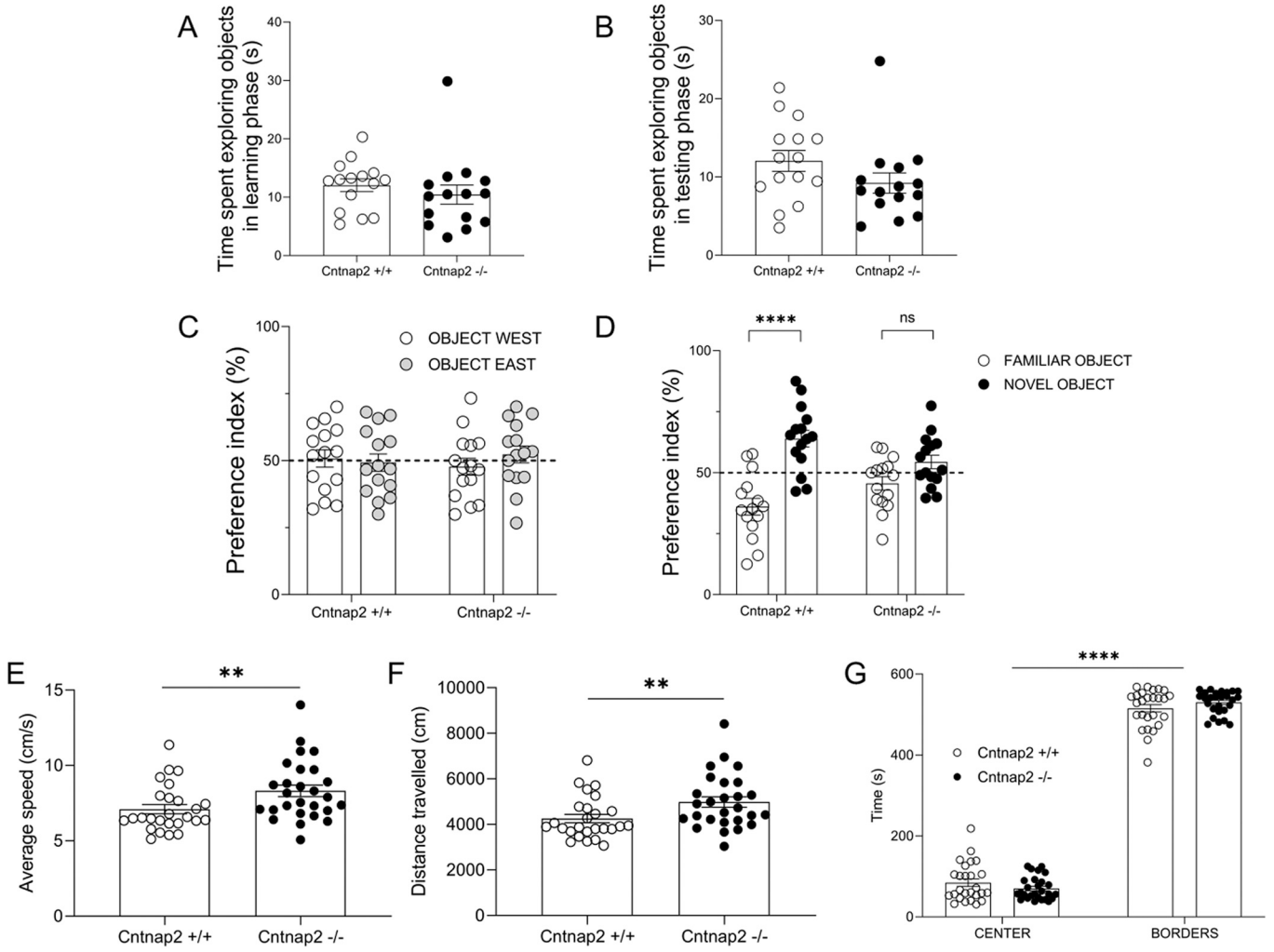

Fig. 3. *Cntnap2*$^{-/-}$ mice exhibit abnormal whisker dependent texture discrimination and general locomotor hyperactivity. *Cntnap2*$^{+/+}$ and *Cntnap2*$^{-/-}$ spent a comparable amount of time exploring objects in both learning phase (*A*) and testing phase (*B*). (*C*—*D*) Quantification of tNORT performance by *Cntnap2*$^{+/+}$ and *Cntnap2*$^{-/-}$ mice. Preference index (%) for familiar objects (*C*) did not differ between *Cntnap2*$^{+/+}$ and *Cntnap2*$^{-/-}$ mice in the learning phase ($p > 0.05$, Tukey's test following two-way ANOVA). In the testing phase, *Cntnap2*$^{-/-}$ mice did not show a preference for the novel textured object, as compared to Shank3b+/+ mice (*D*, ****$p < 0.0001$, Tukey's test following two-way ANOVA). Locomotor hyperactivity in *Cntnap2*$^{-/-}$ mice was assessed in open field arena. *Cntnap2*$^{-/-}$ mice showed higher average speed (E, **$p < 0.01$, Mann-Whitney test) and distance travelled (F, **$p < 0.01$, Mann-Whitney test) in the open field, as compared to controls. Both *Cntnap2*$^{+/+}$ and *Cntnap2*$^{-/-}$ mice spent significantly more time in borders as compared to the center of the arena (G, ****$p < 0.0001$, Tukey's post hoc following two-way ANOVA). All plots report the mean values ± SEM; each dot represents one animal. Genotypes are as indicated ($n = 15$ *Cntnap2*$^{+/+}$ and 15 *Cntnap2*$^{-/-}$ for tNORT test and $n = 26$ *Cntnap2*$^{+/+}$ and 27 *Cntnap2*$^{-/-}$).

cluster-corrected using a cluster threshold of $p = 0.01$, Fig. 2*A*). Unilateral quantifications of rsfMRI signal in regions of interest confirmed functional over-connectivity within the right ($t = 3.11$, $p = 0.005$, Fig. 2*B*, top panel) and left S1 ($t = 3.41$, $p = 0.002$, Fig. 2*B*, bottom panel). To rule out the presence of thalamo-cortical functional connectivity alterations in *Cntnap2* mutants, we carried out voxelwise rsfMRI connectivity mapping of the ventral posterior medial thalamic nucleus (VPM), which receives afferents from whiskers via brainstem nuclei and projects to S1 layer 4 (Petersen, 2007). Our analysis revealed unimpaired rsfMRI of the VPM in *Cntnap2* mutants as compared to wild-type littermates ($t > 2$, $p < 0.05$ and FWER cluster-corrected using a cluster threshold of $p = 0.01$, Fig. 2*C*). Preserved rsfMRI connectivity of the VPM was confirmed by region-wise unilateral quantifications between right SS and VPM ($t = 0.53$, $p = 0.063$, Fig. 1*D*, top panel) and between left SS and VPM ($t = 0.51$, $p = 0.067$, Fig. 2*D*, bottom panel). Our set of functional connectivity analysis also revealed unimpaired rsfMRI connectivity between S1 and VPM, and the TN. Our findings indicate an aberrant over-synchronization within somatosensory areas in *Cntnap2* mutants.

3.2. *Cntnap2*$^{-/-}$ mice show impaired texture discrimination through whiskers

To test whether S1 over-synchronization is accompanied by an altered response to somatosensory stimuli in *Cntnap2* mutants, we tested *Cntnap2*$^{-/-}$and control mice in a whisker-dependent version of tNORT (Balasco et al., 2021) (Fig. 3) using sandpaper-wrapped cylinders that differ only in texture (smooth or rough; see Methods).

Both genotypes spent a comparable total amount of time exploring objects in both the testing and learning phase (unpaired *t*-test, *Cntnap2*$^{+/+}$vs *Cntnap2*$^{-/-}$, $p > 0.05$; Fig. 3*A-B*), indicating that mutant mice have preserved exploration through whiskers. During the tNORT learning phase (Fig. 3*C*) both genotypes did not show any preference for one of the identical textured objects (two-way ANOVA, main effect of objects $F_{(1, 56)} = 7.994e\text{-}030$, $p = 0.9999$). During the test phase, control mice spent a significantly larger amount of time exploring the novel object, testifying a preference in the novel texture exploration through whiskers. Conversely, *Cntnap2*$^{-/-}$mice spent comparable time exploring the novel and the familiar object, (Fig. 3*D*; Tukey's post hoc following two-way ANOVA, familiar object vs novel object within *Cntnap2*$^{+/+}$, $p < 0.0001$ and *Cntnap2*$^{-/-}$, $p = 0.2033$). These results suggest that *Cntnap2*−/− mice display impaired whisker-dependent texture discrimination. No sex differences were found in the preference index during both learning and testing phases (three-way ANOVA, *Cntnap2*$^{+/+}$ vs *Cntnap2*$^{-/-}$, main effect of sex $p > 0.05$ in learning and testing phases).

To exclude that whisker-dependent behavioral responses were due to a general hyporeactivity phenotype, we assessed *Cntnap2*$^{-/-}$ and control mice in an open field arena. *Cntnap2*$^{-/-}$ mice showed a significantly increased average speed (Fig. 3*E*; Mann-Whitney test, *Cntnap2*$^{-/-}$ vs *Cntnap2*$^{+/+}$; $p = 0.0093$) and distance travelled (Fig. 3*F*; Mann-Whitney test, *Cntnap2*$^{-/-}$ vs *Cntnap2*$^{+/+}$; $p = 0.0093$) as compared to wild-type littermates. Both genotypes spent a comparable amount of time in center and borders of the open field arena (Fig. 3*G*; Tukey's post hoc following two-way ANOVA, *Cntnap2*$^{+/+}$ vs *Cntnap2*$^{-/-}$ within center; $p = 0.5150$; *Cntnap2*$^{+/+}$ vs *Cntnap2*$^{-/-}$ within borders; $p = 0.5132$) while having a preference for border regions of the arena (Fig. 3*G*; Tukey's post hoc following two-way ANOVA, center vs borders within *Cntnap2*$^{+/+}$ and center vs borders within *Cntnap2*$^{-/-}$; $p < 0.0001$), indicating a similar level of anxiety. No sex differences were found in the behavior analyzed (two-way ANOVA, *Cntnap2*$^{+/+}$ vs *Cntnap2*$^{-/-}$, main effect of sex $p > 0.05$ for average speed, distance travelled and time spent in center/borders).

3.3. *Cntnap2*$^{-/-}$ mice show increased c-*fos* mRNA expression in S1 following whisker stimulation under anesthesia (WS)

We next investigated c-*fos* mRNA induction in S1 following WS (Fig. 4). WS induced c-*fos* mRNA expression in S1 of both genotypes, as compared to anesthetized unstimulated animals; however, whisker-stimulated *Cntnap2*$^{-/-}$ mice showed a more pronounced c-*fos* induction in S1 (Fig. 4*A*). Quantification of c-*fos* mRNA mean signal intensity confirmed these observations (Fig. 4*B*; Tukey's post hoc following one-way ANOVA, anesthesia *Cntnap2*$^{+/+}$ vs anesthesia *Cntnap2*$^{-/-}$ $p > 0.05$; anesthesia vs. WS $p = 0{,}0001$ in *Cntnap2*$^{+/+}$ and $p < 0{,}0001$ in *Cntnap2*$^{-/-}$; WS *Cntnap2*$^{+/+}$ vs WS *Cntnap2*$^{-/-}$, $p = 0{,}0062$). Quantification of c-*fos* mRNA in S1 layers revealed a similar pattern of induction in L2/3, L4 and L5/6 (Fig. 4*C-E*; Tukey's post hoc following one-way ANOVA, anesthesia vs WS $p < 0{,}0001$ in L2/3, L4, and L5/6). WS instead induced a similar c-*fos* mRNA upregulation in the somatosensory thalamus (VPM; Fig. 5*A*) and hippocampus (Fig. 5*B*) of both *Cntnap2*$^{+/+}$ and *Cntnap2*$^{-/-}$ mice, compared to anesthetized unstimulated animals. No difference in c-*fos* mRNA signal intensity was detected between the two genotypes in other brain regions analyzed, such as motor cortex (Fig. 5*C*), medial thalamic nuclei (Fig. 5*D*) and amygdala (Fig. 5*E*). Given the functional hyper-connectivity and c-*fos* mRNA upregulation found in the S1 of *Cntnap2*$^{-/-}$ mice, we next used RT-qPCR to evaluate the expression of excitatory (vesicular glutamate transporters vGLUT1 and 2) and inhibitory (glutamic acid decarboxylase GAD1 and 2, parvalbumin Pvalb) markers in the neocortex of adult *Cntnap2*$^{+/+}$ and *Cntnap2*$^{-/-}$ adult mice. vGLUT1 and 2 mRNAs were overexpressed in *Cntnap2*$^{-/-}$ mice compared to controls ($^*p < 0.05$ unpaired *t*-test), while mRNA levels of inhibitory markers did not differ between the two genotypes (Fig. 6). These results suggest that an increased excitation/inhibition (E/I) ratio might underlie S1 functional hyperconnectivity and somatosensory discrimination deficits of *Cntnap2* mice.

4. Discussion

In this study, we report that adult *Cntnap2* mutant mice, compared to age-matched controls, display increased functional connectivity within S1, accompanied by impaired whisker-dependent texture discrimination and increased c-*fos* mRNA expression in S1 following whisker stimulation. Increased sensitivity to somatosensory stimulation is consistent with increased E/I balance detected in the *Cntnap2* neocortex.

Both hyper- and hypo-sensitivity to tactile stimuli have been proposed to contribute to social deficits and other autism-related behaviors. Accordingly, sensory abnormalities are a common trait in mice harboring ASD-relevant mutations (Balasco et al., 2019). Previous studies addressed somatosensory deficits in mouse models of ASD (He et al., 2017; Chelini et al., 2019; Chen et al., 2020; Orefice, 2020; Pizzo et al., 2020; Balasco et al., 2021), including *Cntnap2*$^{-/-}$ mice (Peñagarikano et al., 2011; Dawes et al., 2018; Antoine et al., 2019). Mice use their whiskers for a variety of behaviors including conspecifics interaction, exploration and environmental navigation (Ahl, 1986; Brecht, 2007; Diamond et al., 2008; Diamond and Arabzadeh, 2013). Previous studies showed that *Cntnap2*$^{-/-}$ mice display aberrant prefronto-cortical functional connectivity (Liska et al., 2018) and general patterns of hyperconnectivity across major brain structures including the neocortex (Choe et al., 2021). Here we investigated functional synchronization in somatosensory areas of *Cntnap2* mutants. Functional coupling between S1 and other somatosensory areas (VPM and TN) was preserved in mutant mice, while *Cntnap2*$^{-/-}$ mice displayed focal hyperconnectivity within S1 compared to controls (Fig. 2). This data suggests the presence of impaired somatosensory processing in *Cntnap2* mice, pointing out at possible whisker-dependent behavioral deficits in these mutants.

We therefore investigated whisker-dependent responses in *Cntnap2*$^{-/-}$ and control mice. We first used a version of tNORT specifically designed to favor whisker-mediated object exploration (Wu et al.,

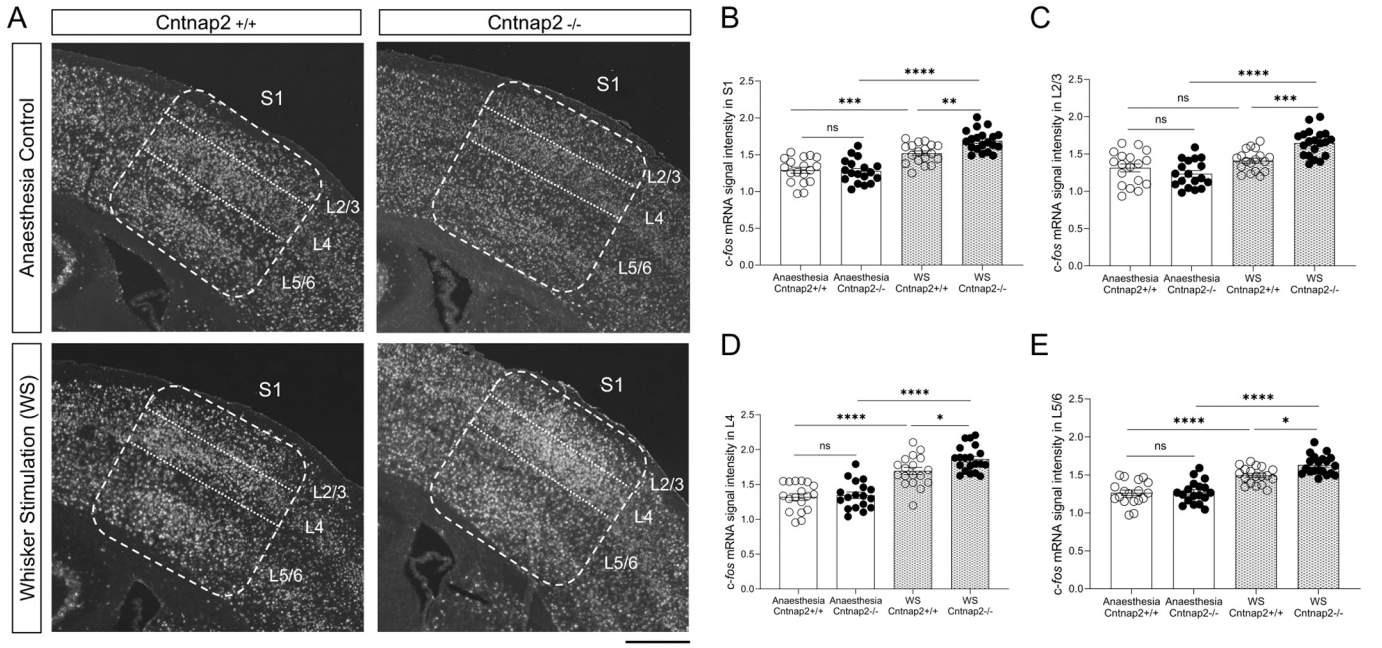

Fig. 4. Increased neuronal activation in S1 of *Cntnap2*$^{-/-}$ mice following whisker stimulation under anesthesia. (*A*). Representative images of c-*fos* mRNA in situ hybridization in S1 (white staining) of *Cntnap2*$^{+/+}$ and *Cntnap2*$^{-/-}$ mice, 20 min following anesthesia only or whisker stimulation under anesthesia (WS). Scale bar: 500 μm. (*B*) Quantification of c-*fos* mRNA signal intensity in S1. (*C-E*) Quantification of c-*fos* mRNA signal intensity in S1 layers 2/3 (*C*), 4 (*D*), and 5/6 (*E*). Values are expressed as mean normalized signal intensities ± SEM (n = 4–8 sections from 3 animals per genotype). **p < 0.01, ***p < 0.001, ****p < 0.0001. Genotypes and treatments are as indicated. Abbreviations: S1, primary somatosensory cortex; L2–6, S1 cortical layers.

2013; Balasco et al., 2021). As compared with control animals, *Cntnap2* mutant mice were not able to discriminate between objects with different textures, though spending the same amount of time investigating objects with identical texture (Fig. 3). These results indicate that *Cntnap2*$^{-/-}$ mice display a reduced ability to discriminate different texture using their whiskers. To the best of our knowledge, this is the first evidence of aberrant whisker-dependent texture discrimination in *Cntnap2*$^{-/-}$ mice. Behavioral hyporeactivity to whisker stimulation would not be attributable to a generalized hypoactive phenotype, since *Cntnap2* mutants showed hyperlocomotion in the open field arena (Fig. 3), as previously described in mice (Peñagarikano et al., 2011) and CDFE patients (Strauss et al., 2006).

Recent studies performed in mice lacking ASD-associated genes showed that repetitive whisker stimulation modulates the expression of the immediate-early gene *c-fos* in several brain areas, including S1 (Chelini et al., 2019; Pizzo et al., 2020; Balasco et al., 2021). Most importantly, a recent study using two complementary whole-brain mapping approaches (rsfMRI and c-Fos-iDISCO+ imaging) showed a high degree of correlation between activity-induced c-Fos expression and functional connectivity maps in *Cntnap2* mice, indicating that c-Fos expression mapping is a good proxy of functional connectivity in this ASD model (Choe et al., 2021). In keeping with these findings, c-*fos* mRNA upregulation observed in *Cntnap2*$^{-/-}$ S1 following WS (Fig. 4) might reflect the hyperconnectivity pattern detected in this sensory area by rsfMRI (Fig. 2). Moreover, the preserved connectivity between S1 and VPM (Fig. 2) and the stronger whisker-dependent c-*fos* mRNA induction (detected in S1 but not in other brain areas; Figs. 4 and 5) suggest that abnormal whisker-dependent responses observed in *Cntnap2*$^{-/-}$ mice mostly depend of local circuit dysfunction within S1.

Spontaneous seizures were reported in *Cntnap2* $^{-/-}$ mice over 6 months of age (Peñagarikano et al., 2011), a phenotype shared with CDFE patients (Strauss et al., 2006). Accordingly, we detected increased expression of excitatory but not inhibitory neuron markers in the neocortex of *Cntnap2* mice (Fig. 6), confirming the increased E/I balance previously detected in these mutants (Antoine et al., 2019). Thus, the enhanced c-*fos* induction detected in the *Cntnap2* S1 following WS (Fig. 3) might also depend on the hyperexcitable phenotype of *Cntnap2* mutant mice. However, none of our animals tested exceeded 6 months of age, nor showed signs of epileptic seizures. Moreover, c-*fos* mRNA signal intensity in other brain regions analyzed following WS tests did not show any difference between genotypes (Fig. 5), thus excluding the possibility that heightened c-*fos* mRNA expression was related to a generalized hyperexcitability in this model.

GABAergic interneuron defects in *Cntnap2*$^{-/-}$ mice (Peñagarikano et al., 2011; Gao et al., 2018) might account for the increased neuronal activation within the S1 of *Cntnap2*$^{-/-}$ mice following whisker stimulation. Increased excitation/inhibition (E/I) ratio has been proposed as a common mechanism underlying the core features of ASDs (Rubenstein and Merzenich, 2003; Nelson and Valakh, 2015; Lee et al., 2017; Bozzi et al., 2018; Sohal and Rubenstein, 2019). Although recent data suggest that E/I imbalance might be a compensatory mechanism rather than the underlying cause (Antoine et al., 2019), acute changes in E/I ratio have been reported to both induce or reduce ASD phenotypes (Yizhar et al., 2011; Selimbeyoglu et al., 2017). Increased excitability in the somatosensory cortex was indeed observed in young *Cntnap2*$^{-/-}$ mice, in spite of reduced whisker-evoked spiking (Antoine et al., 2019). Our data (Fig. 6) support the idea that E/I imbalance in the *Cntnap2* neocortex is mostly due to a deregulated expression of excitatory but not inhibitory markers. Accordingly, other authors reported no change in GAD and Pvalb expression in the *Cntnap2* neocortex (Lauber et al., 2018).

Previous studies showed that asynchronous firing patterns are present in S1 cortical neurons of *Cntnap2*$^{-/-}$ mice (Peñagarikano et al., 2011), accompanied by reduced dendritic spine density and impaired oscillations (Lazaro et al., 2019). This is in line with our data showing c-*fos* upregulation in S1 of *Cntnap2* $^{-/-}$ mice following WS (Fig. 4). Moreover, these findings indicate a broad network dysfunction within S1 in these mutants. It is generally accepted that cognitive function relies on coordinated interactions within and across discrete neuronal networks, and several studies point to a long- and short-range disconnectivity within brain areas both in ASD patients (Müller and Fishman, 2018) and mouse models (Zerbi et al., 2021). Indeed, long-range functional connectivity is disrupted in *Cntnap2*$^{-/-}$ mice (Liska et al.,

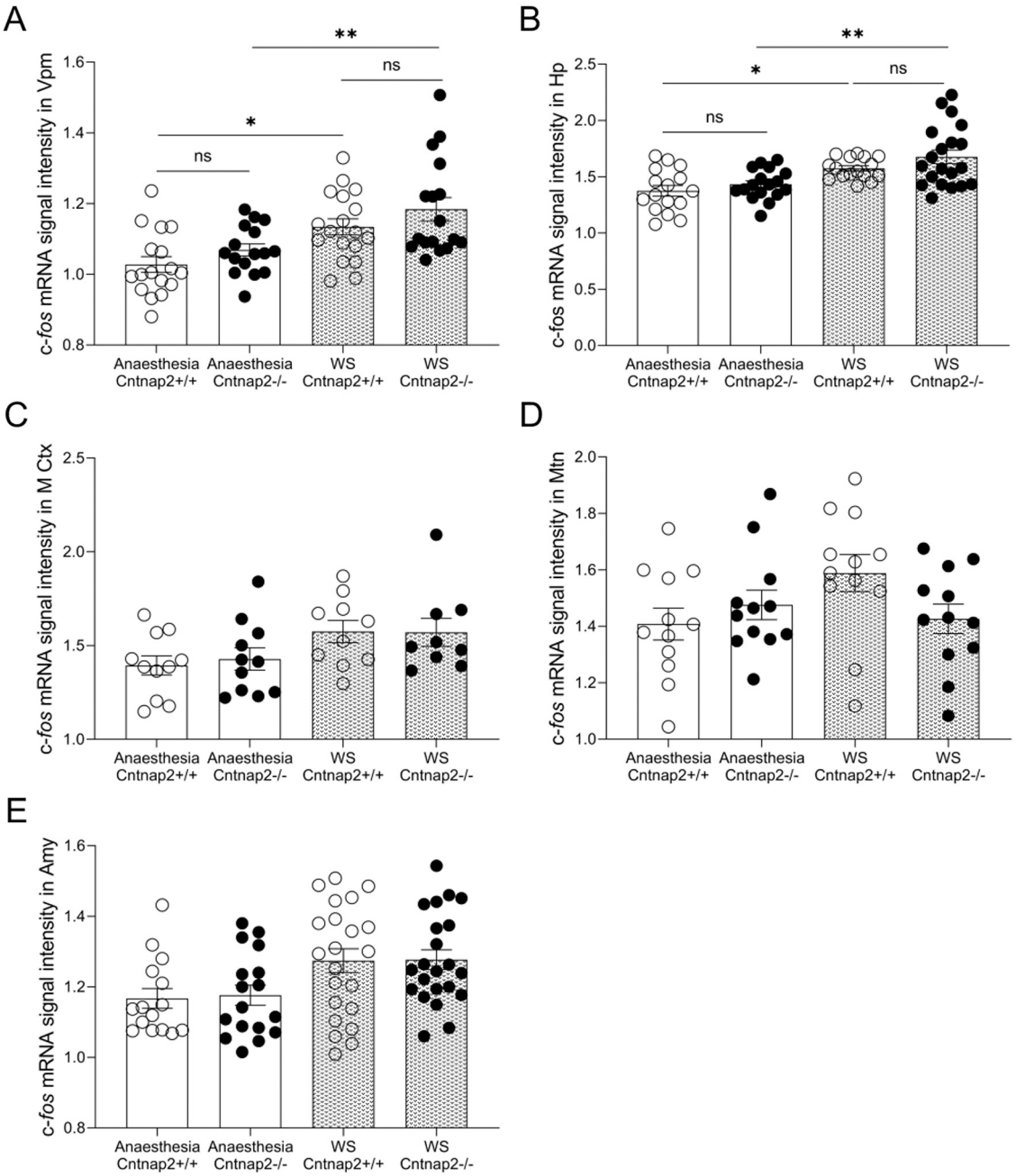

Fig. 5. c-*fos* mRNA expression in other brain regions from *Cntnap2*$^{+/+}$ and *Cntnap2*$^{-/-}$ mice following whisker stimulation under anesthesia (WS) or anesthesia only. (*A, B*) c-*fos* mRNA upregulation was detected in the ventral postero-medial nucleus of the thalamus (Vpm, *A*) and hippocampus (Hp, *B*) of *Cntnap2*$^{-/-}$ and control mice following WS. (*C-E*) *Cntnap2*$^{+/+}$ and *Cntnap2*$^{-/-}$ mice did not show any difference in c-*fos* mRNA in motor cortex (M Ctx, *C*), medial thalamic nuclei (Mtn, *D*) and amygdala (Amy, *E*) in the two experimental conditions. Values are expressed as mean signal intensities ±SEM. *$p < 0.05$ **p < 0.01, Tukey post-hoc test following one-way-ANOVA (n = 2–8 sections from 3 animals per genotype). Genotypes and treatments are as indicated.

2018) and human subjects bearing *Cntnap2* polymorphisms (Scott-Van Zeeland et al., 2010). In this context, the focal hyperconnectivity within S1 found in *Cntnap2*$^{-/-}$ mice (Fig. 2) might represent a functional substrate for altered sensory processing in this model.

5. Conclusions

Our data support the concept that impaired cortical processing of sensory information may contribute to behavioral deficits in *Cntnap2* mice. However, some limitations have to be acknowledged. First, at this stage the present study does not provide insights on the mechanisms responsible for the behavioral and circuit dysfunctions here reported. Secondly, since this study focuses on adult animals, it remains to be elucidated whether these defects appear early during development. Further studies are needed to fill these gaps and assess whether altered processing of sensory information within sensory hubs represents a common deficit in mice harboring ASD-related mutations.

Funding

YB is supported by the Strategic Project TRAIN - Trentino Autism Initiative (https://projects.unitn.it/train/index.html) from the University of Trento (grant 2018–2022) and the Autism Research Institute (ARI research award 2021). LB is a recipient of a PhD fellowship from the

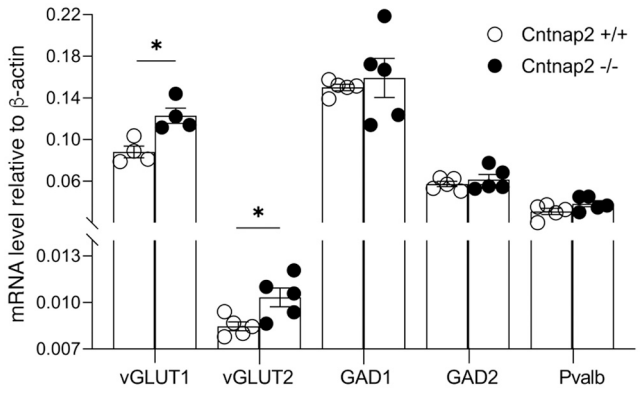

Fig. 6. Expression of excitatory and inhibitory neuron markers in the neocortex of *Cntnap2*$^{-/-}$ mice. Quantification of vGLUT1, vGLUT2, GAD1, GAD2, and Pvalb mRNA expression (RT-qPCR) in the neocortex of adult *Cntnap2*$^{+/+}$ and *Cntnap2*$^{-/-}$mice. For both genotypes, the expression level of each mRNA of interest was normalized on the expression of the β-actin reference gene, and the relative expression of each target was calculated (mean ± SEM of at least 4 replicates from pools of 5 animals per genotype; each dot represents a technical replicate; *p < 0.05 unpaired t-test).

University of Trento and CARITRO Foundation (Trento, Italy). LP is supported by the University of Trento (postdoctoral fellowship and starting grant for young researchers). GC is supported by a post-doctoral fellowship from the CARITRO Foundation (Trento, Italy). GP was supported by the Brain and Behavior Research Foundation (NARSAD Young Investigator Grant; ID: 26617) and the University of Trento (Starting Grant for Young Researchers). A. Gozzi was funded by the Simons Foundation (SFARI 400101), Brain and Behavior Foundation (NARSAD - National Alliance for Research on Schizophrenia and Depression), the European Research Council (ERC-DISCONN, GA802371), the NIH (1R21MH116473-01A1) and the Telethon Foundation (GGP19177).

CRediT authorship contribution statement

Luigi Balasco: Conceptualization, Formal analysis, Investigation, Methodology, Visualization, Writing – original draft, Writing – review & editing. **Marco Pagani:** Conceptualization, Data curation, Formal analysis, Investigation, Methodology, Software, Writing – original draft. **Luca Pangrazzi:** Investigation. **Gabriele Chelini:** Formal analysis, Investigation, Methodology. **Francesca Viscido:** Investigation, Writing – review & editing. **Alessandra Georgette Ciancone Chama:** Investigation. **Alberto Galbusera:** Investigation, Methodology. **Giovanni Provenzano:** Formal analysis, Funding acquisition, Investigation, Writing – review & editing. **Alessandro Gozzi:** Conceptualization, Data curation, Formal analysis, Funding acquisition, Writing – review & editing. **Yuri Bozzi:** Conceptualization, Formal analysis, Funding acquisition, Supervision, Visualization, Writing – original draft, Writing – review & editing.

Acknowledgments

YB dedicates this paper to the memory of his friend and colleague Matteo Caleo, Professor of Physiology at the University of Padova (Italy). His kindness, passion, and scientific integrity will remain as an example for future generations of scientists. The authors thank the technical and administrative staff of CIMeC, CIBIO, and IIT for assistance.

References

Ahl, A.S., 1986. The role of vibrissae in behavior: A status review. Vet. Res. Commun. 10, 245–268.
Alarcón, M., Abrahams, B.S., Stone, J.L., Duvall, J.A., Perederiy, J.V., Bomar, J.M., Sebat, J., Wigler, M., Martin, C.L., Ledbetter, D.H., Nelson, S.F., Cantor, R.M., Geschwind, D.H., 2008. Linkage, association, and gene-expression analyses identify CNTNAP2 as an autism-susceptibility gene. Am. J. Hum. Genet. 82, 150–159.
American Psychiatric Association, 2013. Diagnostic and Statistical Manual of Mental Disorders: DSM-5. American Psychiatric Association, Arlington, VA.
Anderson, G.R., Galfin, T., Xu, W., Aoto, J., Malenka, R.C., Südhof, T.C., 2012. Candidate autism gene screen identifies critical role for cell-adhesion molecule CASPR2 in dendritic arborization and spine development. Proc. Natl. Acad. Sci. U. S. A. 109, 18120–18125.
Antoine, M.W., Langberg, T., Schnepel, P., Feldman, D.E., 2019. Increased excitation-inhibition ratio stabilizes synapse and circuit excitability in four autism mouse models. Neuron 101, 648–661.e644.
Arakawa, H., Erzurumlu, R.S., 2015. Role of whiskers in sensorimotor development of C57BL/6 mice. Behav. Brain Res. 287, 146–155.
Arking, D.E., Cutler, D.J., Brune, C.W., Teslovich, T.M., West, K., Ikeda, M., Rea, A., Guy, M., Lin, S., Cook, E.H., Chakravarti, A., 2008. A common genetic variant in the neurexin superfamily member CNTNAP2 increases familial risk of autism. Am. J. Hum. Genet. 82, 160–164.
Bakkaloglu, B., O'roak, B.J., Louvi, A., Gupta, A.R., Abelson, J.F., Morgan, T.M., Chawarska, K., Klin, A., Ercan-Sencicek, A.G., Stillman, A.A., Tanriover, G., Abrahams, B.S., Duvall, J.A., Robbins, E.M., Geschwind, D.H., Biederer, T., Gunel, M., Lifton, R.P., State, M.W., 2008. Molecular cytogenetic analysis and resequencing of contactin associated protein-like 2 in autism spectrum disorders. Am. J. Hum. Genet. 82, 165–173.
Balasco, L., Provenzano, G., Bozzi, Y., 2019. Sensory abnormalities in autism spectrum disorders: a focus on the tactile domain, from genetic mouse models to the clinic. Front Psychiatry 10, 1016.
Balasco, L., Pagani, M., Pangrazzi, L., Chelini, G., Ciancone Chama, A.G., Shlosman, E., Mattioni, L., Galbusera, A., Iurilli, G., Provenzano, G., Gozzi, A., Bozzi, Y., 2021. Abnormal whisker-dependent behaviors and altered cortico-hippocampal connectivity in Shank3b−/− mice. Cereb Cortex bhab 399.
Ben-Sasson, A., Cermak, S.A., Orsmond, G.I., Tager-Flusberg, H., Carter, A.S., Kadlec, M. B., Dunn, W., 2007. Extreme sensory modulation behaviors in toddlers with autism spectrum disorders. Am. J. Occup. Ther. 61, 584–592.
Bozzi, Y., Provenzano, G., Casarosa, S., 2018. Neurobiological bases of autism-epilepsy comorbidity: a focus on excitation/inhibition imbalance. Eur. J. Neurosci. 47, 534–548.
Brecht, M., 2007. Barrel cortex and whisker-mediated behaviors. Curr. Opin. Neurobiol. 17, 408–416.
Chelini, G., Zerbi, V., Cimino, L., Grigoli, A., Markicevic, M., Libera, F., Robbiati, S., Gadler, M., Bronzoni, S., Miorelli, S., Galbusera, A., Gozzi, A., Casarosa, S., Provenzano, G., Bozzi, Y., 2019. Aberrant somatosensory processing and connectivity in mice lacking Engrailed-2. J. Neurosci. 39, 1525–1538.
Chen, Q., Deister, C.A., Gao, X., Guo, B., Lynn-Jones, T., Chen, N., Wells, M.F., Liu, R., Goard, M.J., Dimidschstein, J., Feng, S., Shi, Y., Liao, W., Lu, Z., Fishell, G., Moore, C.I., Feng, G., 2020. Dysfunction of cortical GABAergic neurons leads to sensory hyper-reactivity in a Shank3 mouse model of ASD. Nat. Neurosci. 23, 520–532.
Choe, K.Y., Bethlehem, R.A.I., Safrin, M., Dong, H., Salman, E., Li, Y., Grinevich, V., Golshani, P., Denardo, L.A., Peñagarikano, O., Harris, N.G., Geschwind, D.H., 2021. Oxytocin normalizes altered circuit connectivity for social rescue of the Cntnap2 knockout mouse. Neuron. 110, 795–808.
Coletta, L., Pagani, M., Whitesell, J.D., Harris, J.A., Bernhardt, B., Gozzi, A., 2020. Network structure of the mouse brain connectome with voxel resolution. Sci. Adv. 6 (eabb7187).
Dawes, J.M., Weir, G.A., Middleton, S.J., Patel, R., Chisholm, K.I., Pettingill, P., Peck, L. J., Sheridan, J., Shakir, A., Jacobson, L., Gutierrez-Mecinas, M., Galino, J., Walcher, J., Kühnemund, J., Kuehn, H., Sanna, M.D., Lang, B., Clark, A.J., Themistocleous, A.C., Iwagaki, N., West, S.J., Werynska, K., Carroll, L., Trendafilova, T., Menassa, D.A., Giannoccaro, M.P., Coutinho, E., Cervellini, I., Tewari, D., Buckley, C., Leite, M.I., Wildner, H., Zeilhofer, H.U., Peles, E., Todd, A.J., Mcmahon, S.B., Dickenson, A.H., Lewin, G.R., Vincent, A., Bennett, D.L., 2018. Immune or genetic-mediated disruption of CASPR2 causes pain hypersensitivity due to enhanced primary afferent excitability. Neuron 97, 806–822.
Di Martino, A., Yan, C.G., Li, Q., Denio, E., Castellanos, F.X., Alaerts, K., Anderson, J.S., Assaf, M., Bookheimer, S.Y., Dapretto, M., Deen, B., Delmonte, S., Dinstein, I., Ertl-Wagner, B., Fair, D.A., Gallagher, L., Kennedy, D.P., Keown, C.L., Keysers, C., Lainhart, J.E., Lord, C., Luna, B., Menon, V., Minshew, N.J., Monk, C.S., Mueller, S., Müller, R.A., Nebel, M.B., Nigg, J.T., O'Hearn, K., Pelphrey, K.A., Peltier, S.J., Rudie, J.D., Sunaert, S., Thioux, M., Tyszka, J.M., Uddin, L.Q., Verhoeven, J.S., Wenderoth, N., Wiggins, J.L., Mostofsky, S.H., Milham, M.P., 2014. The autism brain imaging data exchange: towards a large-scale evaluation of the intrinsic brain architecture in autism. Mol. Psychiatry 19, 659–667.
Diamond, M.E., Arabzadeh, E., 2013. Whisker sensory system - from receptor to decision. Prog. Neurobiol. 103, 28–40.
Diamond, M.E., Von Heimendahl, M., Knutsen, P.M., Kleinfeld, D., Ahissar, E., 2008. 'Where' and 'what' in the whisker sensorimotor system. Nat. Rev. Neurosci. 9, 601–612.
Erzurumlu, R.S., Gaspar, P., 2020. How the barrel cortex became a working model for developmental plasticity: a historical perspective. J. Neurosci. 40, 6460–6473.
Foss-Feig, J.H., Heacock, J.L., Cascio, C.J., 2012. Tactile responsiveness patterns and their association with core features in autism spectrum. Res. Autism Spectr. Disord. 6, 337–344.
Gao, R., Piguel, N.H., Melendez-Zaidi, A.E., Martin-De-Saavedra, M.D., Yoon, S., Forrest, M.P., Myczek, K., Zhang, G., Russell, T.A., Csernansky, J.G., Surmeier, D.J.,

Penzes, P., 2018. CNTNAP2 stabilizes interneuron dendritic arbors through CASK. Mol. Psychiatry 23, 1832–1850.
Gordon, A., Salomon, D., Barak, N., Pen, Y., Tsoory, M., Kimchi, T., Peles, E., 2016. Expression of Cntnap2 (Caspr2) in multiple levels of sensory systems. Mol. Cell. Neurosci. 70, 42–53.
He, C.X., Cantu, D.A., Mantri, S.S., Zeiger, W.A., Goel, A., Portera-Cailliau, C., 2017. Tactile defensiveness and impaired adaptation of neuronal activity in the Fmr1 knock-out mouse model of autism. J. Neurosci. 37, 6475–6487.
Lauber, E., Filice, F., Schwaller, B., 2018. Dysregulation of parvalbumin expression in the Cntnap2−/− mouse model of autism spectrum disorder. Front. Mol. Neurosci. 11, 262.
Lazaro, M.T., Taxidis, J., Shuman, T., Bachmutsky, I., Ikrar, T., Santos, R., Marcello, G. M., Mylavarapu, A., Chandra, S., Foreman, A., Goli, R., Tran, D., Sharma, N., Azhdam, M., Dong, H., Choe, K.Y., Peñagarikano, O., Masmanidis, S.C., Rácz, B., Xu, X., Geschwind, D.H., Golshani, P., 2019. Reduced prefrontal synaptic connectivity and disturbed oscillatory population dynamics in the CNTNAP2 model of autism. Cell Rep. 27, 2567–2578.
Lee, E., Lee, J., Kim, E., 2017. Excitation/inhibition imbalance in animal models of autism spectrum disorders. Biol. Psychiatry 81, 838–847.
Liska, A., Bertero, A., Gomolka, R., Sabbioni, M., Galbusera, A., Barsotti, N., Panzeri, S., Scattoni, M.L., Pasqualetti, M., Gozzi, A., 2018. Homozygous loss of autism-risk gene CNTNAP2 results in reduced local and long-range prefrontal functional connectivity. Cereb. Cortex 28, 1141–1153.
Mammen, M.A., Moore, G.A., Scaramella, L.V., Reiss, D., Ganiban, J.M., Shaw, D.S., Leve, L.D., Neiderhiser, J.M., 2015. Infant avoidance during a tactile task predicts autism spectrum behaviors in toddlerhood. Infant Ment. Health J. 36, 575–587.
Müller, R.A., Fishman, I., 2018. Brain connectivity and neuroimaging of social networks in autism. Trends Cogn. Sci. 22, 1103–1116.
Nelson, S.B., Valakh, V., 2015. Excitatory/inhibitory balance and circuit homeostasis in autism spectrum disorders. Neuron 87, 684–698.
Orefice, L.L., 2020. Peripheral somatosensory neuron dysfunction: emerging roles in autism spectrum disorders. Neuroscience 445, 120–129.
Pagani, M., Damiano, M., Galbusera, A., Tsaftaris, S.A., Gozzi, A., 2016. Semi-automated registration-based anatomical labelling, voxel based morphometry and cortical thickness mapping of the mouse brain. J. Neurosci. Methods 267, 62–73.
Pagani, M., Barsotti, N., Bertero, A., Trakoshis, S., Ulysse, L., Locarno, A., Miseviciute, I., De Felice, A., Canella, C., Supekar, K., Galbusera, A., Menon, V., Tonini, R., Deco, G., Lombardo, M.V., Pasqualetti, M., Gozzi, A., 2021. mTOR-related synaptic pathology causes autism spectrum disorder-associated functional hyperconnectivity. Nat. Commun. 12, 6084.
Peñagarikano, O., Abrahams, B.S., Herman, E.I., Winden, K.D., Gdalyahu, A., Dong, H., Sonnenblick, L.I., Gruver, R., Almajano, J., Bragin, A., Golshani, P., Trachtenberg, J. T., Peles, E., Geschwind, D.H., 2011. Absence of CNTNAP2 leads to epilepsy, neuronal migration abnormalities, and core autism-related deficits. Cell 147, 235–246.
Petersen, C.C.H., 2007. The functional organization of the barrel cortex. Neuron 56, 339–355.
Pizzo, R., Lamarca, A., Sassoè-Pognetto, M., Giustetto, M., 2020. Structural bases of atypical whisker responses in a mouse model of CDKL5 deficiency disorder. Neuroscience 445, 130–143.
Poliak, S., Gollan, L., Martinez, R., Custer, A., Einheber, S., Salzer, J.L., Trimmer, J.S., Shrager, P., Peles, E., 1999. Caspr2, a new member of the neurexin superfamily, is localized at the juxtaparanodes of myelinated axons and associates with K+ channels. Neuron 24, 1037–1047.
Poliak, S., Salomon, D., Elhanany, H., Sabanay, H., Kiernan, B., Pevny, L., Stewart, C.L., Xu, X., Chiu, S.Y., Shrager, P., Furley, A.J., Peles, E., 2003. Juxtaparanodal clustering of shaker-like K+ channels in myelinated axons depends on Caspr2 and TAG-1. J. Cell Biol. 162, 1149–1160.
Robertson, C.E., Baron-Cohen, S., 2017. Sensory perception in autism. Nat. Rev. Neurosci. 18, 671–684.
Rubenstein, J.L.R., Merzenich, M.M., 2003. Model of autism: increased ratio of excitation/inhibition in key neural systems. Genes Brain Behav. 2, 255–267.
Schmucker, C., Seeliger, M., Humphries, P., Biel, M., Schaeffel, F., 2005. Grating acuity at different luminances in wild-type mice and in mice lacking rod or cone function. Invest. Ophthalmol. Vis. Sci. 46, 398–407.
Scott-Van Zeeland, A.A., Abrahams, B.S., Alvarez-Retuerto, A.I., Sonnenblick, L.I., Rudie, J.D., Ghahremani, D., Mumford, J.A., Poldrack, R.A., Dapretto, M., Geschwind, D.H., Bookheimer, S.Y., 2010. Altered functional connectivity in frontal lobe circuits is associated with variation in the autism risk gene CNTNAP2. Sci. Transl. Med. 2, 56ra80.
Selimbeyoglu, A., Kim, C.K., Inoue, M., Lee, S.Y., Hong, A.S.O., Kauvar, I., Ramakrishnan, C., Fenno, L.E., Davidson, T.J., Wright, M., Deisseroth, K., 2017. Modulation of prefrontal cortex excitation/inhibition balance rescues social behavior in CNTNAP2-deficient mice. Sci. Transl. Med. 9.
Sgadò, P., Provenzano, G., Dassi, E., Adami, V., Zunino, G., Genovesi, S., Casarosa, S., Bozzi, Y., 2013. Transcriptome profiling in engrailed-2 mutant mice reveals common molecular pathways associated with autism spectrum disorders. Molecular Autism 4, 51.
Sinclair, D., Oranje, B., Razak, K.A., Siegel, S.J., Schmid, S., 2017. Sensory processing in autism spectrum disorders and fragile X syndrome - from the clinic to animal models. Neurosci. Biobehav. Rev. 76, 235–253.
Sohal, V.S., Rubenstein, J.L.R., 2019. Excitation-inhibition balance as a framework for investigating mechanisms in neuropsychiatric disorders. Mol. Psychiatry 24, 1248–1257.
Strauss, K.A., Puffenberger, E.G., Huentelman, M.J., Gottlieb, S., Dobrin, S.E., Parod, J. M., Stephan, D.A., Morton, D.H., 2006. Recessive symptomatic focal epilepsy and mutant contactin-associated protein-like 2. N. Engl. J. Med. 354, 1370–1377.
Wu, H.P., Ioffe, J.C., Iverson, M.M., Boon, J.M., Dyck, R.H., 2013. Novel, whisker-dependent texture discrimination task for mice. Behav. Brain Res. 237, 238–242.
Yizhar, O., Fenno, L.E., Prigge, M., Schneider, F., Davidson, T.J., O'shea, D.J., Sohal, V.S., Goshen, I., Finkelstein, J., Paz, J.T., Stehfest, K., Fudim, R., Ramakrishnan, C., Huguenard, J.R., Hegemann, P., Deisseroth, K., 2011. Neocortical excitation/inhibition balance in information processing and social dysfunction. Nature 477, 171–178.
Zerbi, V., Pagani, M., Markicevic, M., Matteoli, M., Pozzi, D., Fagiolini, M., Bozzi, Y., Galbusera, A., Scattoni, M.L., Provenzano, G., Banerjee, A., Helmchen, F., Basson, M. A., Ellegood, J., Lerch, J.P., Rudin, M., Gozzi, A., Wenderoth, N., 2021. Brain mapping across 16 autism mouse models reveals a spectrum of functional connectivity subtypes. Mol. Psychiatry 26, 7610–7620.